Recovering EEG brain signals: Artifact suppression with wavelet enhanced independent component analysis

Nazareth P. Castellanos, Valeri A. Makarov*

Neuroscience Laboratory, Department of Applied Mathematics, Escuela de Óptica, Universidad Complutense de Madrid, Avda. Arcos de Jalón s/n, 28037 Madrid, Spain

Abstract

Independent component analysis (ICA) has been proven useful for suppression of artifacts in EEG recordings. It involves separation of measured signals into statistically independent components or sources, followed by rejection of those deemed artificial. We show that a "leak" of cerebral activity of interest into components marked as artificial means that one is going to lost that activity. To overcome this problem we propose a novel wavelet enhanced ICA method (wICA) that applies a wavelet thresholding not to the observed raw EEG but to the demixed independent components as an *intermediate* step. It allows recovering the neural activity present in "artificial" components. Employing semi-simulated and real EEG recordings we quantify the distortions of the cerebral part of EEGs introduced by the ICA and wICA artifact suppressions in the time and frequency domains. In the context of studying cortical circuitry we also evaluate spectral and partial spectral coherences over ICA/wICA-corrected EEGs. Our results suggest that ICA may lead to an underestimation of the neural power spectrum and to an overestimation of the coherence between different cortical sites. wICA artifact suppression preserves both spectral (amplitude) and coherence (phase) characteristics of the underlying neural activity.

1. Introduction

Nowadays in the medical practice the Fourier transform (FT) and spectral coherence (SC) are the mathematical methods most widely used for the analysis of electro-encephalo-graphic recordings (EEGs). The FT allows studying local (*univariate*) spectral density of the EEG power across different frequency bands. The SC is a *bivariate* characteristic that determines the degree of synchrony of oscillations recorded at a pair of electrodes. It allows inferring on the presence and strength of functional association between the corresponding cortical areas, thus providing a rough insight on the cortical circuitry. For three (or more) simultaneously recorded (*multivariate*) EEG signals, partial spectral coherence (PSC) extends the limits of the SC, discriminating direct from indirect connections (Brillinger, 1981; Bendat and Piersol, 1986).

A direct use of any of the above mentioned tools with "raw" EEG recordings is strongly restricted by the presence of artifacts

(from eye movements, blinking, muscle activity, etc.), whose magnitude may be much higher than that of the neural signal. Currently, a widely used way to get rid of artifacts is manual or semi-automatic selection of artifact free data segments or epochs. Although in many cases being practical, this artifact rejection procedure is subjective, requires a high skill of the operator and leads to a great decrease of the amount of data available for the subsequent analysis. As an example, from a 10 min long EEG of a healthy subject, one usually obtains roughly a minute of joined artifact free data. In the medical practice a massive presence of artifacts in, e.g. EEGs of children (Tran et al., 2004) or patients with certain injuries (Urrestarazu et al., 2004) makes the data reduction even higher and strongly limits the efficiency of this procedure and is an obstacle for a reliable diagnosis on the basis of the above mentioned derived characteristics. Besides the data reduction, segmentation leads to other issues like data stationarity across distant epochs, cerebral activity during or including artifact episodes. Hence, employing a non-cutting (filtering-like) procedure for data cleaning becomes even more attractive.

An EEG recording from a single scalp electrode can be considered as a mixture of signals from different brain regions and

---

* Corresponding author. Tel.: +34 913946900; fax: +34 913946885.
  E-mail address: vmakarov@opt.ucm.es (V.A. Makarov).

artifacts. In the first approximation signals of the neural origin can be considered independent on artifacts [for details see, e.g. (Jung et al., 2000b; James and Hesse, 2005)]. With this in mind recently a non-cutting method of artifact suppression based on independent component analysis (ICA) has been proposed (Bell and Sejnowski, 1995). Later several modifications of the original algorithm have been introduced (Anemüller et al., 2003; James and Gibson, 2003; James and Lowe, 2003; Joyce et al., 2004; Flexer et al., 2005; Melissant et al., 2005). ICA tries to separate the recorded EEG signals into statistically independent sources (components), and then rejects those responsible for artifacts. The majority of EEG applications of ICA focus on the removal of ocular artifacts, where it has been shown to be very useful (Vigario, 1997; Jung et al., 2000a,b; Tong et al., 2001; Joyce et al., 2004; Flexer et al., 2005). Currently ICA is perceived as a potentially robust and powerful method for the artifact removal in EEG data and receives an increasing attention (Jung et al., 2000a,b; Vigario et al., 2000; Tong et al., 2001; Iriarte et al., 2003; Tran et al., 2004; Urrestarazu et al., 2004). However, there are still several issues that should be addressed:

(a) The identification of components responsible for artifacts requires experience of the operator and a priori knowledge about the artifact structure. Besides, an optimal algorithm application is achieved with relatively short (around 10 s) data segments (Jung et al., 2000a). This counterintuitive result: "more data are not always better" has been discussed, e.g. in (Brown et al., 2001) and it assumes a laborious sequential analysis of EEG divided into many short epochs. As a step towards an automatic artifact removal, James and Gibson (2003) proposed to use independent components constrained to be similar to some reference signal incorporating a priori information on the artifact temporal structure. Another approach for detection of the components responsible for ocular artifacts uses correlation between electro-oculograms and independent components (Flexer et al., 2005).

(b) While ICA is now considered an important technique for removing artifacts in EEG signals, there are still little quantitative results showing its advantages and limitations. Existing studies have focused almost exclusively on the spectral improvements provided by ICA decomposition when suppressing typical artifacts. Although it has been proven that ICA-corrected EEGs exhibit a strong reduction in the spectral bands corresponding to artifacts (Tong et al., 2001; Tran et al., 2004), recently there has appeared an alert that the artifact suppression may also corrupt the power spectrum of the underlying neural activity (Wallstrom et al., 2004; Kierkels et al., 2006). Thus the question: how the ICA-correction distorts the spectrum of the underlying cerebral activity needs to be quantitatively studied.

(c) One of the challenging applications of EEGs is the study of cortical circuitry and its reorganization as the brain state changes [see, e.g. (Rodriguez et al., 1999; von Stein et al., 1999; Varela et al., 2001)]. The current literature lacks evaluation of ICA artifact suppression for analysis of synchrony between different electrodes. The non-local characteristics

like spectral and partial spectral coherences depend on the phase relation between signals recorded at different electrodes. Thus coherence distortions due to artifacts and their rejection in general are not reducible to the power (amplitude) spectrum distortions. Hence for a reliable circuitry analysis, the coherence distortion should also be quantified.

Another popular technique of the signal analysis is the wavelet transform (WT) (Mallat, 1998). It allows signal decomposition on multiple scales with further analysis of the wavelet coefficients, and for instance suppression of some of them resembling "undesirable" properties in the signal. The WT has been used for analysis of EEGs from the very beginning in different contexts: detection of seizure (Schiff et al., 1994); characterization of epilepsy (Goelz et al., 2000; Alegre et al., 2003; Mormann et al., 2005); study of event-related potentials (Quiroga and Garcia, 2003; Makinen et al., 2004) and mental tasks (Murata, 2005); separation of fetal ECG from mother ECG (Mochimaru et al., 2004); reduction of ballistocardiogram artifacts (Wan et al., 2006), etc. Recently, Rong-Yi and Zhong (2005) showed that wavelet denoising of raw EEG may improve performance of the following ICA decomposition.

In this paper we first provide a novel method for artifact suppression in EEG recordings: wavelet enhanced ICA (wICA). The method relies on ICA and makes use of wavelet thresholding not for denoising of the observed raw EEG but as an *intermediate* step to the demixed independent components. The thresholding allows conservation of the time-frequency structure of artifacts and recovering of the cerebral activity "leaked" into the components. Then we quantify distortions introduced by the conventional ICA and wICA methods in the time and frequency domains with semi-simulated and real EEG recordings. Finally, with the perspective of studying cortical circuitry we, for the first time, provide results on spectral and partial spectral coherences evaluated over ICA- and wICA-corrected EEGs.

2. Materials and methods

2.1. EEG recordings

EEG data were acquired following standard guidelines (Privik et al., 1993) from healthy subjects with the eyes open. We used the ECI Electro—Cap System with 19 scalp electrodes placed according to the International 10–20 System. The signals were digitized at a rate of 256 Hz and further filtered (notch filter at 50 Hz, and band pass filter 4–45 Hz).

2.2. Semi-simulated data

We manually cut out of a real EEG artifact free non-overlapping epochs collecting this way 15 s clean signals. Then we simulate eye blinking and heart beat artifacts and mix them with the clean EEG accounting for the artifact morphology, spatial distribution, and scalp topographies using mixing matrix from a real recording (Hori et al., 2004; Delorme et al., 2005). To reproduce the shape of eye blinking episodes we use a band pass

filtered (1–3 Hz) Poisson random process of 0.3 s per episode. The heart beat is simulated by a pulse train at 1 Hz.

2.3. Spectrum estimation

We use a multi-taper Fourier transform for continuous data sets. The algorithm reduces the variance of spectral estimate by using a set of tapers rather than a unique data taper or spectral window. It is especially effective for short data segments (Thomson, 1982; Percival and Walden, 1993). A MatLab toolbox is freely available at http://chronux.org/chronux(Jarvis and Mitra, 2001).

2.4. Inferring on functional connectivity

To infer on the topological structure of the interaction between different brain regions a common approach uses spectral coherence (SC) and partial spectral coherence (PSC). To evaluate the SC and PSC we use a MatLab toolbox available at http://bci.tugraz.at/~schloegl/matlab/eeg/gdf4/.

2.4.1. Spectral coherence

The SC is a normalized measure of the cross-spectrum $P_{xy}(\omega) = P_x(\omega)P_y^*(\omega)$ of two EEG signals, $x(t)$ and $y(t)$, recorded at different sites:

$$SC_{xy}(\omega) = \frac{P_{xy}(\omega)}{\sqrt{P_{xx}(\omega)P_{yy}(\omega)}}. \tag{1}$$

If the SC equals to zero for all frequencies, ω, the two processes are linearly independent, i.e. no interaction between the two measured EEG signals exists. $|SC| = 1$ indicates a perfect linear relationship between the two processes, i.e. the dynamics of one signal is completely explained by the other. A *significant* (see Section 2.4.3) level of the SC between these extremes, $0 \leq |SC| \leq 1$, in a certain frequency band means association (in terms of synchronization) between the signals and it is a sign of the functional connectivity between the corresponding cortical areas.

2.4.2. Partial spectral coherence

The PSC of two EEG signals, $x(t)$ and $y(t)$, is given by:

$$PSC_{xy|C}(\omega) = -\frac{g_{xy}(\omega)}{\sqrt{g_{yy}(\omega)g_{xx}(\omega)}}, \tag{2}$$

where $g(\omega) = P^{-1}(\omega)$ is the inverse matrix of the cross-spectra, and C denotes all the other signals. The PSC is also a bounded function, $0 \leq |PSC| \leq 1$. To decide whether two sites are (functionally) coupled *directly* or not, we apply the same criterion as for the SC.

2.4.3. Surrogate data test

To conclude positively on the connectivity (synchrony) between two EEG channels the coherence (either SC or PSC) should be higher than the significance level obtained under assumption of the null hypothesis that time series are statistically independent. In other words we have to estimate the level of random leak between the channels. To evaluate the significance

level we use surrogate data test (Theiler et al., 1992; Schreiber and Schmitz, 2000). The surrogate time series are obtained from the original by randomizing phase relations keeping intact other first order characteristics (Korzeniewska et al., 2003).

2.5. ICA based artifact suppression

ICA is based on the three following assumptions: (i) experimental data is a spatially stable mixture of the activities of temporarily independent cerebral and artifactual sources, (ii) the superposition of potentials arising from different parts of the brain, scalp, and body is linear at the electrodes, and propagation delays from the sources to the electrodes are negligible, and (iii) the number of sources is no bigger than the number of electrodes.

ICA starts assuming that K simultaneously recorded EEG signals $X(t) = \{x_1(t), \ldots, x_K(t)\}$ are linear mixtures of N ($N \leq K$) a priori unknown independent components (sources) $S(t) = \{s_1(t), \ldots, s_N(t)\}$ including artifactual and of the neural origin:

$$X(t) = MS(t), \tag{3}$$

where M is the unknown mixing matrix defining weights at which each source is present in the EEG signals recorded at the scalp. Topography scalp maps of the components provide additional information on the localization of the sources. The aim of ICA is to estimate both $S(t)$ and M from $X(t)$. We use infomax algorithm proposed by Bell and Sejnowski (1995) and further modified by Amari et al. (1996) and Lee et al. (1999). The algorithm is implemented in EEGLAB MatLab toolbox (Delorme and Makeig, 2004) available at http://sccn.ucsd.edu/eeglab. It uses neural networks maximizing the joint entropy and minimizing the mutual information among the output components of a neural processor. For crosschecking we also employ another ICA implementation, FastICA (Hyvärinen and Pajunen, 1999), available at http://www.cis.hut.fi/projects/ica/fastica.

Once the algorithm has been applied we analyze the temporal structure and topography of the components $S(t)$ (e.g. the ocular artifacts mainly project to frontal sites) and identify among them those components that account for artifacts. Then we set the identified artifactual components to zero, $s_{artf}(t) = 0$, obtaining a new component matrix $\hat{S}(t)$ where the artifactual sources have been rejected. Finally, we reconstruct ICA-corrected EEG signals as:

$$\hat{X}(t) = M\hat{S}(t). \tag{4}$$

Obtained this way the new data set $\hat{X}(t)$ represents the ICA estimation of the original, artifact free data.

2.6. Wavelet enhanced ICA (wICA) artifact removal

Let us now introduce our method that uses Wavelet technique to enhance the performance of the ICA artifact suppression method.

When dealing with real EEGs, ICA estimated independent components capturing artificial sources, besides of strongly present artifacts, frequently contain a considerable amount of
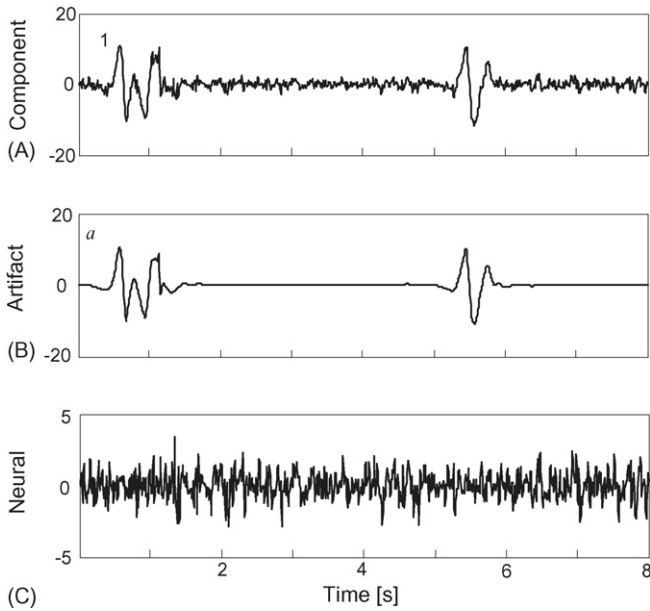
Fig. 1. Decomposition of an independent component into artifactual and neural parts. (A) The independent component found by ICA has two episodes of eye blinking (around 0.8 and 5.5 s). (B) Artifactual source presented in the component. (C) Underlying signal of the neural origin leaked into the component.

cerebral activity. The later may occur, e.g. due to the limitation on the maximal number of independent sources, restriction on temporal independence or suboptimal algorithm application (Jung et al., 2000a; Brown et al., 2001). Rejection of such components supposes a loss of a part of the cerebral activity and, consequently, distortion of the artifact free EEG (Friston, 1998). Fig. 1A illustrates the first independent component, $s_1(t)$, found by ICA and identified as corresponding to blinking artifacts. According to the ICA assumptions this component cannot include other artifacts independent of the ocular. The component can be split into a high amplitude artifact $a(t)$ (Fig. 1B) and a low amplitude residual neural signal $n(t)$ (Fig. 1C):

$$s_1(t) = a(t) + n(t). \tag{5}$$

Note that the ocular artifact vanishes outside of the blinking episodes (Fig. 1B), however, the component has a significant amount of the persisting neural signal (Fig. 1A–C).

In the conventional ICA algorithm the whole component is set to zero $s_1(t) = 0$ before the signal recomposition, Eq. (4). This way in the ICA-corrected EEG we lose a part of the cerebral activity:

$$\hat{x}_j(t) = r_j(t) - m_{j1}n(t), \tag{6}$$

where $r_j(t) = x_j(t) - m_{j1}a(t)$ is the artifact free signal and m_{j1} is the corresponding weight from the mixing matrix, M.

Estimating the persisting neural signal $n(t)$ we can further subtract it from the component and thus correct the ICA reconstruction of the artifact free EEG recording. A priori, as it happens in ICA, the decomposition (5) of the independent component into artifactual and neural activity is unknown. However, using properties of the signals $a(t)$ and $n(t)$ we can estimate them. Indeed, the artifact, $a(t)$, has high magnitude (power) and is localized in the time and/or in frequency domains, while $n(t)$

is of low amplitude and has a broad band spectrum (Fig. 1B and C). These properties fit well with the wavelet decomposition technique that provides an optimal resolution both in the time and frequency domains, without requiring the signal stationarity.

The continuous wavelet transform of the independent component $s_1(t)$ (somehow similar to the Fourier transform) reads:

$$W^s(d, b) = \frac{1}{\sqrt{d}} \int s_1(t)\psi_{d,b}(t)\,dt, \quad \psi_{d,b} = \psi\left(\frac{t-b}{d}\right), \quad (7)$$

where $W^s(d, b)$ is the wavelet representation of $s_1(t)$, ψ is the mother wavelet with b and d defining the time localization and scale. The WT (7) is redundant and therefore in practice its discrete counterpart (DWT) is usually used (a MatLab package is available at http://www.dsp.rice.edu/software). In the DWT the time scales and localizations take only fixed values, usually $d = 2^j$, $b = k2^j$ with integers j and k playing roles of the decomposition level and temporal localization at this level, respectively. Using Eqs. (5) and (7) we can write:

$$W^s(d, b) = W^a(d, b) + W^n(d, b), \tag{8}$$

where $W^a(d, b)$ and $W^n(d, b)$ are the wavelet coefficients obtained by the transformation (7) of the artificial and neural parts of the component, respectively. As above mentioned the coefficients corresponding to artifacts will be of high amplitude and well localized in time and scales, while the neural coefficients will be distributed across all scales, and will have a wide spectrum of low energy. To illustrate this we apply the continuous WT (7) to the three signals shown in Fig. 1. Fig. 2 shows the independent component and its parts in the wavelet space. Indeed, the artificial component, $a(t)$, has high amplitude wavelet coefficients (Fig. 2B) localized in time windows of the blinking episodes (see also Fig. 1), and in long enough scales. The neural part, $n(t)$, is small and spreads homogeneously over the whole spectrum of scales and localizations. Accordingly, the decomposition procedure (5) can be generally described as a thresholding: all wavelet coefficients above a certain threshold are set to zero, and then the resulting structure is used for the
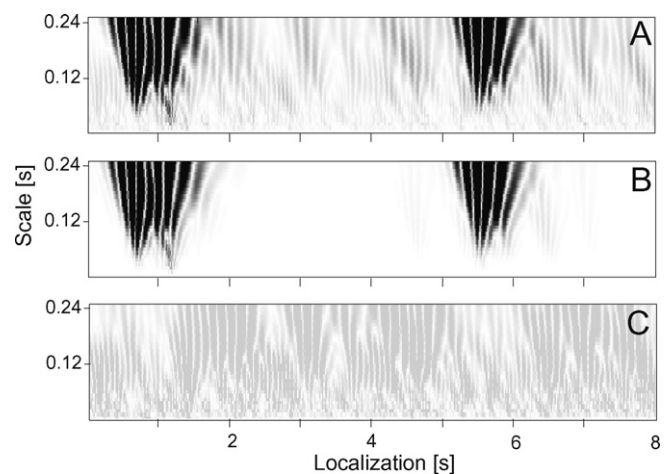
Fig. 2. Wavelet representation of the independent component $s_1(t)$ (A) and its parts: artifactual $a(t)$ (B), and neural $n(t)$ (C). Gray intensity codifies the absolute value of wavelet coefficients. The data corresponds to the voltage traces shown in Fig. 1.

inverse wavelet transformation. Note that the thresholding can only be performed with the DWT, where in addition to (8) we get separation of the wavelet coefficients into "artificial" and "neural", i.e. if $W^a(j, k) = 0$ then $W^n(j, k) \neq 0$ and vice versa. The described procedure is very much similar to the denoising technique proposed by Donoho et al. (1995) but here we aim at the contrary goal: separate useful low amplitude and broad band signal from the strong artifacts.

Finally the wavelet enhanced ICA (wICA) algorithm for artifact suppression in EEG is:

(1) Apply a conventional ICA decomposition to raw EEG thus obtaining the mixing matrix M and N independent components $\{s_1(t), s_2(t), \ldots, s_N(t)\}$.
(2) Wavelet transform components obtaining their representations $\{W(j, k)\}_{s_i}$.
(3) Threshold the wavelet coefficients, i.e. set $W(j, k) = 0$ for those that are higher than the threshold, $|W(j, k)| > K$.
(4) Inverse wavelet transform of the thresholded coefficients $W(j, k)$ thus recomposing components consisting sources of the neural origin only $\{n_i(t)\}$.
(5) Compose wICA-corrected EEG: $\tilde{X}(t) = M \cdot [n_1(t), n_2(t), \ldots, n_N(t)]^{\mathrm{T}}$.

Selection of the threshold value, K, is an essential element of the algorithm. Here we use the simplest fixed form threshold:

$$K = \sqrt{2 \log N}\sigma, \tag{9}$$

where N is the length of the data segment to be processed, and $\sigma^2 = \mathrm{median}(|W(d, b)|)/0.6745$ is the estimator of the magnitude of the neural wide band signal part. As we shall see further such threshold yields a good performance with ocular and heart beat artifacts. Other thresholding strategies (see review in, e.g. (Debnath, 2002)) can also be applied, possibly providing better tuning of the algorithm to the particular peculiarities of other artifacts or EEGs. Note that our algorithm may be completely automatic, since no laborious visual inspection of the independent components followed by selection of those of them responsible for artifacts is required. The components having no high magnitude artifacts just pass through the wavelet thresholding (steps 2–4) intact ($n_k(t) = s_k(t)$). This allows an automatic algorithm application, and consequently its most crucial step 1, to relatively short (say around 10 s) contiguous epochs as suggested by Jung et al. (2000a).

The wICA algorithm has been realized in MatLab and is available upon request.

3. Results

We assess the performance of artifact suppression by the ICA and wICA methods when applying them to EEGs with two final goals: (1) test the quality of recovering of the brain signals under artifacts; (2) quantify the distortions of the EEG power spectrum and spectral coherences introduced by ICA and wICA.

For the first test we employ semi-simulated recordings where a priori information on the cerebral signals allows estimation of the recovering quality in the time domain. For the second goal

we use real EEGs. As a reference, in the later case, we use artifact free non-overlapping epochs between consecutive blinks manually delimited off-line in the original EEG recordings by a careful inspection of the channel traces (Jung et al., 2000b) in such a way that the other artifacts are not present in the selected electrodes (e.g. FP1). Further on we shall refer to these epochs as control. Once suitable data (ICA/wICA corrected EEGs and control epochs) have been obtained, posterior spectral and connectivity analyzes are applied. Then we compare the derived characteristics (power spectra, coherences) obtained over the same epochs in ICA and wICA corrected EEGs with those found for the control.

3.1. Suppression of artifacts by ICA and wICA methods

Let us first illustrate artifact suppression on an example of rejection of eye blinking and heart beat artifacts. The eye blinking artifact appears in EEG as big pulses well localized in time and has the strongest impact to EEG signals. The heart beat artifact appears when an electrode is placed nearby an artery and it shows up as a train of short lasting, relatively low amplitude pulses at frequency about 70 beats per minute. Fig. 3A shows an example of EEG taken from a healthy adult subject instructed to stay at a steady state with the eyes open. The shown data segment has both artifact types we interest in. Two eye blinking episodes (localized around 3 and 7 s) spread over all channels and affect most strongly the frontal sites (from FP1 to F8). Control segments (for FP1) are taken between consecutive artifact episodes, e.g. at 3.5–6.5 s. The heart beat artifact contaminates mostly left tempo-occipital electrodes (T3, T5, O1).

The ICA algorithm separates contribution of the artifactual and neural signals into 19 independent components. The first independent component exhibits strong pulses (Fig. 3B) and projects mainly to frontal sites (Fig. 3C). This coincides with the "fingerprints" of blinking artifacts whose morphology is characterized by strong short lasting pulses and scalp topography shows a clear evidence in the frontal sites (Jung et al., 2000a). Using this a priori knowledge we identify the first component as a responsible of the eye blinking artifacts. Similarly, the fourth independent component (Fig. 3B) captures the rhythmic pulses from the heart beat artifact. It projects to the left tempo-occipital area (Fig. 3C).

Now according to the ICA artifact suppression method we set the first and the fourth components to zero and reconstruct the EEG recording using Eq. (4), thus obtaining ICA-corrected EEG (Fig. 4A). Note that this way in accordance with the ICA assumptions we aim to suppress heart beat and ocular artifacts only. We also clean the same EEG by the wICA algorithm. Here we skip the manual analysis of the components, but instead apply the automatic wavelet thresholding (steps 2–4) followed by the signal recomposition (step 5). Fig. 4B shows EEG corrected by wICA.

Visual inspection of the cleaned EEGs confirms that both methods effectively suppress both artifact types. However, analyzing signals first at the frontal electrodes within artifact free epochs (outside of blinking episodes) we observe some distortions introduced by the ICA method. The EEG signal cleaned
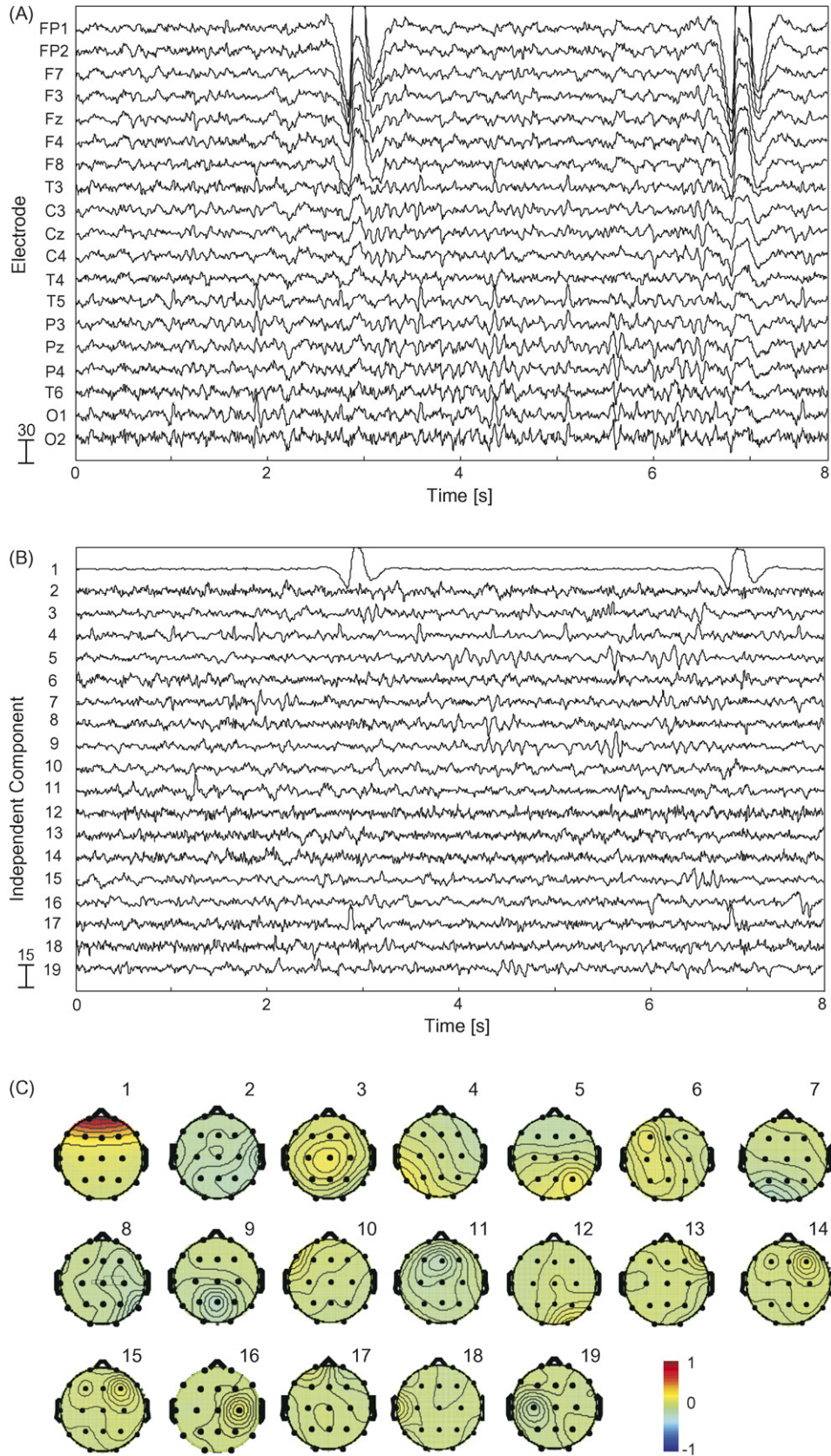
Fig. 3. An example of ICA decomposition of EEG contaminated by ocular and heart beat artifacts. (A) Original EEG data (a segment of 8 s is shown). (B) Independent components decomposing the original EEG into 19 sources. The first component is identified as responsible of the ocular artifacts, while the fourth captures the heart beat artifacts. (C) Scalp maps showing relative projection strengths of the components over all electrodes. Artifactual components "#1" and "#4" project most strongly to the frontal and left tempo-occipital areas, respectively.
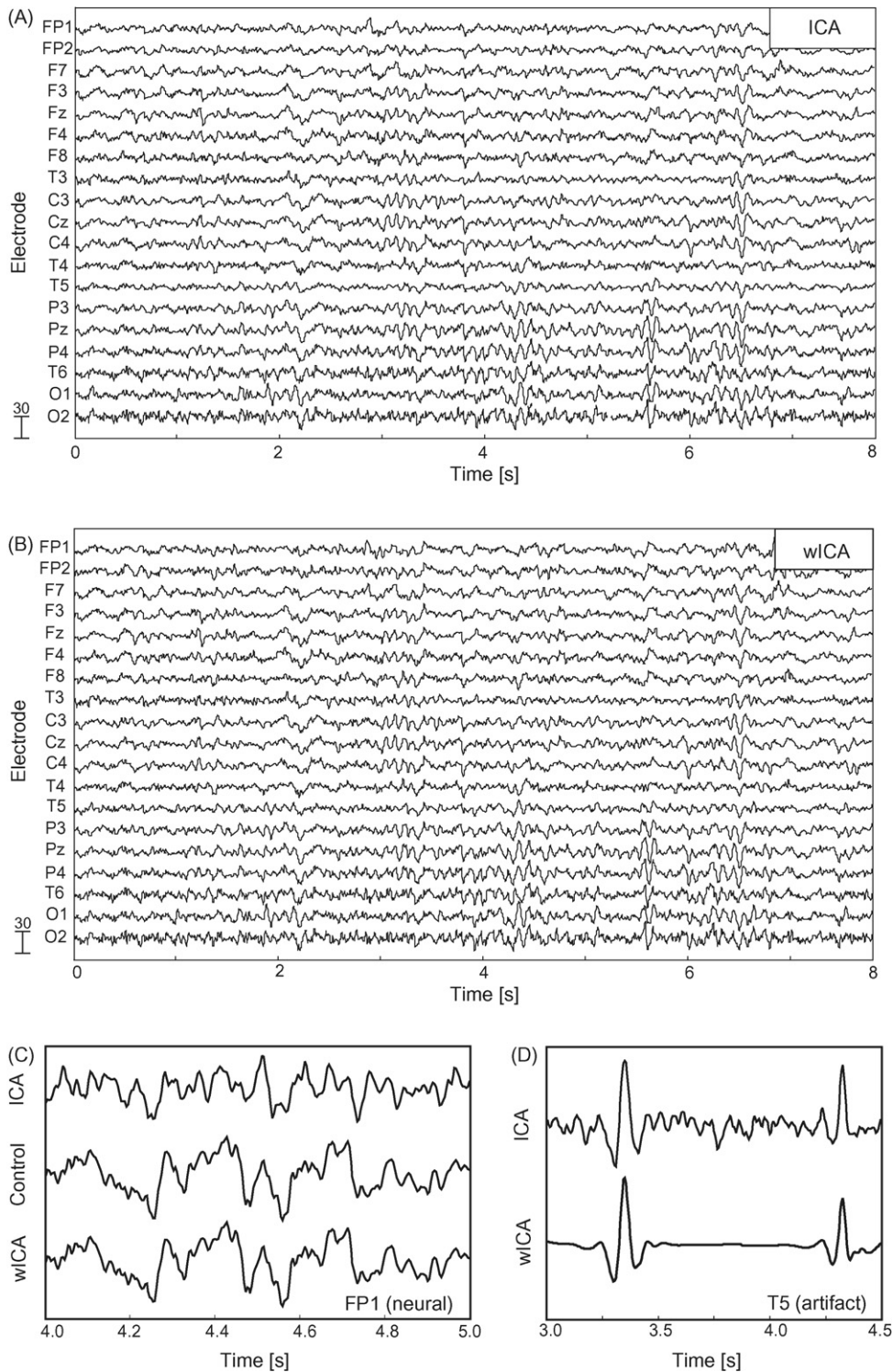
Fig. 4. Artifact suppression and signal distortion by ICA and wICA methods. (A and B) Ocular and heart beat artifacts are effectively suppressed by the ICA (A) and wICA (B) methods (compare to Fig. 3A). (C) Zoomed signals during a control (artifact free) epoch at FP1 electrode. wICA cleaned signal practically reproduces the control signal, while ICA introduces some signal distortions. (D) Estimation of the heart beat artifact delved into T5 electrode according to (11).

by wICA matches well the control, artifact free signal (Fig. 4C). Quantifying the mean squared error in the time domain:

$$\mathrm{MSE} = E[(x_{\mathrm{ICA/wICA}}(t) - x_{\mathrm{control}}(t))^2], \qquad (10)$$

we get for FP1 10.6 and 0.1 μV^2 for ICA and wICA, respectively. To characterize the quality of the heart beat correction by

the both methods we reconstructed the heart beat artifact at T5 electrode:

$$a_{\mathrm{heart\ beat}}(t) = x_{\mathrm{raw}}(t) - \hat{x}_{\mathrm{ICA/wICA}}(t). \qquad (11)$$

Fig. 4D shows the artifact estimations provided by both methods. The artifact reconstructions by ICA and wICA retain about 4.1

and 0.5 μV^2 of the cerebral activity, respectively. We recall that this activity is lost in the corrected EEG.

To discard a possible fault of a particular realization of the ICA algorithm or oddness of the data set we repeated the same procedure employing two different ICA algorithms (Informax and FastICA) and using different EEG recordings (including recordings where only ocular artifacts have been present). Consistently with other studies (McKeown et al., 1998; Brown et al., 2001) both ICA algorithms applied to different recordings gave similar results. Thus we conclude that ICA and wICA methods effectively suppress ocular and heart beat artifacts, but wICA conserves much better the cerebral activity outside of the artifact episodes.

3.2. Recovering brain signal under artifacts

Above we saw that ICA may alter the brain signals, while wICA visually preserves better the brain activity. Let us now quantify in the time domain the distortions introduced by the methods when recovering the brain signals under artifacts.

We generate semi-simulated EEG data by mixing joined preselected artifact free epochs from a real EEG of a healthy subject at rest, and two types of simulated artifacts: ocular and heart beat. The mixture conforms to the artifact morphologies and spatial distributions. Fig. 5A shows an example of such recording. The ocular artifacts propagate through frontal sites, and the heart beat is mostly present in F8 channel. Following the above discussed procedure we calculate 19 independent components (Fig.
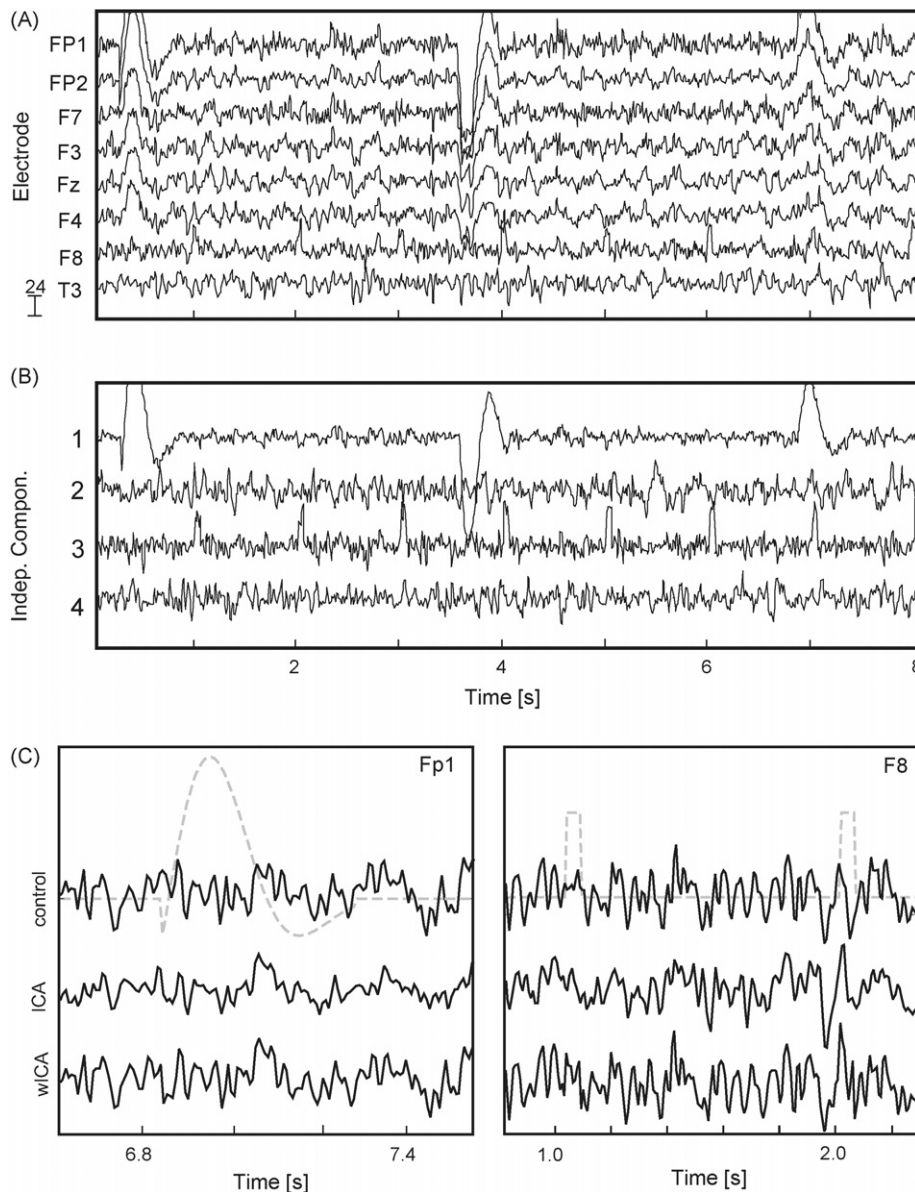
Fig. 5. Recovering of the brain signal under artifacts on semi-simulated EEG. (A) EEG segment of 8 s exhibiting ocular (electrodes FP1–F4) and heart beat (electrode F8) artifacts (the first 8 of 19 channels are shown). (B) Independent components as found by ICA (the first 4 of 19 components are shown). Components #1 and #3 correctly grasp the time courses of ocular and heart beat artifacts, respectively. However, a considerable amount of cerebral activity leaks into these components. (C) Zoomed control and ICA/wICA cleaned signals within ocular (left, FP1) and heart beat (right, F8) artifact episodes. Time courses of simulated artifacts are shown by dashed gray curves. For both artifact types ICA-corrected signals deviate from the reference signals considerably stronger than the wICA cleaned traces.

Table 1
Mean squared error for ICA- and wICA-corrected EEGs in time domain

	FP1 channel (μV^2)	F8 channel (μV^2)
Not corrected	92.4	11.2
ICA	9.9	7.5
wICA	1.6	2.3

The first row (not corrected) quantifies the composite strength of ocular and heart beat artifacts presented in channels FP1 and F8. Each column shows the error in the corresponding channel after artifact suppression by ICA and wICA.

5B), and identify the components number 1 and 3 as artificial, responsible for eye blinking and heart beat, respectively. Note that as above mentioned outside of the artifact episodes the components consist of a considerable amount of cerebral activity that also persists in them during the artifact episodes. This persistent activity degrades the quality of cleaning by ICA. wICA allows recovering of this activity thus enhancing the signal cleaning performance. Fig. 5C illustrates zoomed cerebral activity, simulated artifacts and ICA/wICA recovered signals. Similar to Fig. 4C we observe more prominent signal distortion introduced by the ICA method relative to the distortion by wICA. This holds for suppression of both ocular and heart beat artifacts.

To quantify the quality of recovering of cerebral signals we calculate the mean squared residual error between the reference (artifact free) EEG in channels FP1 and F8 and those obtained after ICA/wICA processing. Table 1 summarizes the results. The presence of ocular and heart beat artifacts in the semi-simulated EEG (Not corrected) is characterized by 92.4 and 11.2 μV^2 in the "recorded" signals relative to the control for FP1 and F8 electrodes, respectively. EEG cleaning by ICA strongly (about nine times) reduces the presence of artifacts in FP1 channel and moderately (one and half times) in F8 channel. This corresponds to 19.4 and 3.5 dB reduction of ocular and heart beat artifacts, respectively. wICA further improves the quality of artifact suppression and enhances performance of ICA by six times in separation of the cerebral activity from ocular artifacts and by more than three times in the case of heart beat artifacts. Thus for wICA we have 35.2 and 13.7 dB reduction of ocular and heart beat artifacts, respectively.

3.3. Power spectrum distortion

Let us now study on real EEG recordings distortions in the power spectrum of the cerebral activity introduced by the artifact suppression.

Signal distortions above quantified (see Table 1) in general will have an effect on the power spectrum of the cerebral signal:

$$P_{\bar{x}\bar{x}}(\omega) = P_{rr}(\omega) + \Delta P(\omega), \tag{12}$$

where P_{rr} is the reference power spectrum of the artifact free signal, $P_{\bar{x}\bar{x}}$ the spectrum of the signal processed either by ICA or wICA, and ΔP is the spectrum distortion introduced by the methods as a side effect, which ideally should be equal to zero.

Assuming that the artifacts are expressed in the first independent component (as shown in Fig. 3), the power spectrum distortion of the signal at the j-th electrode introduced by ICA is given by (Appendix A):

$$\Delta P_j(\omega) = -m_{j1}^2 P_{nn}(\omega). \tag{13}$$

where m_{j1} is the corresponding weight from the mixing matrix M, and P_{nn} is the spectrum of the cerebral activity persisting in the independent component (5). According to (13) the power spectra at all electrodes of the ICA-corrected EEG are underestimated with the same spectral function, P_{nn}, but with different factors, m_{j1}^2. Since m_{j1}^2 decays with j for ocular artifacts (Fig. 3C), the spectral distortions are higher in the frontal sites. The wICA algorithm drastically reduces the residual cerebral activity in the artificial component, consequently it strongly decreases P_{nn}, and thus provides potentially a better approximation of the power spectrum of artifact free EEGs.

To quantify the degree of spectral distortions introduced by the artifact suppression methods across different frequency bands, we calculate the mean power density averaging over ten epochs and convert it to decibels, for the control (reference) segments before and after ICA and wICA artifact suppression. We repeat the same procedure changing the length of the data segments used for ICA decomposition, but keeping the same time boundaries of the control epochs. Table 2 summarizes the results. The spectrum distortion by ICA (difference between the power densities evaluated over ICA-corrected and artifact free signals) increases with the length of the data segment used for estimation of the mixing matrix and independent components. With respect to frequencies, the Theta and Alpha bands are less affected, while Beta and Gamma suffer more. wICA preserves the signal better within the artifact free time windows, and achieves a considerably lower error of the spectrum estimates. Slight distortions are observed in the Theta band, while in the other bands spectral densities are very close to the control values. We also observe a small decrease of the performance with the increase of the segment length used for evaluation of the independent compo-

Table 2
Mean power density in FP1 channel evaluated for the control and after artifact suppression by ICA and wICA using the same data epochs

Frequency band	Power density (dB) control	Artifact rejection method	Segment length for evaluation of independent components, Power density (dB)				
			4 s	8 s	10 s	15 s	25 s
Theta (4–8 Hz)	21.0	ICA	18.8	16.7	16.6	15.9	15.5
		wICA	20.5	20.4	20.3	19.8	18.9
Alpha (8–13 Hz)	17.9	ICA	16.4	14.2	14.1	13.4	13.2
		wICA	17.8	17.7	17.7	17.6	17.5
Beta (13–30 Hz)	16.1	ICA	13.2	11.7	11.8	10.5	10.3
		wICA	16.1	16.0	16.0	16.0	15.9
Gamma (> 30 Hz)	8.6	ICA	5.2	3.6	3.8	2.4	2.1
		wICA	8.6	8.7	8.7	8.7	8.6

Fig. 6. Spectral coherence for a pair of electrodes FP1 and F7 evaluated for the control; and after ICA and wICA artifact suppression. Gray curves depict levels of statistical significance. ICA-corrected EEG shows an overestimated coherence.

nents. To keep this controlled we suggest to use segments of no more than 15 s long. Fixing it at 10 s (the recommended value for ICA decomposition) we get the absolute values of the spectral distortion:

$$|\Delta P| = |P_{ICA/wICA} - P_{cntr}|, \tag{14}$$

over the Theta, Alpha, Beta and Gamma bands at 4.4, 3.8, 4.3 and 4.8 dB for ICA; and 0.7, 0.2, 0.1, and 0.1 dB for wICA. Note that, as we predicted in (13) the spectrum of the ICA-corrected EEG is always lower than the control spectrum.

3.4. Artifact suppression and non-local characteristics derived from EEG

Now let us study how the artifact suppression affects results of infering on interaction (circuitry) between different sites. In the simplest case, synchrony between different electrodes can be grasp by evaluation of spectral and partial spectral coherences (SC and PSC).

Fig. 6 shows an example of the SC evaluated for the pair of electrodes FP1 and F7 at control conditions (using artifact free epochs), and after ICA and wICA artifact suppression. At each graph we also plot the level of statistical significance obtained through the surrogate data test. Coherence in a given frequency band above the surrogate level is considered significant and we conclude on a functional association between these channels.

The coherence calculated over ICA-corrected EEG is significantly higher than the control over all frequency bands (Fig. 6A and B). This overestimation may lead to a spurious hiper-connectivity, i.e. to a false positive conclusion on interaction between the corresponding cortical areas. Artifact suppression by the wICA algorithm offers less amplitude and phase distortions of the cerebral part of EEG and we obtain the coherence estimate very close to the control conditions (Fig. 6A and C).

Let us now test how the results of artifact suppression affects the identification of connectivity patterns between EEG signals. To conclude positively on the presence of a connection between a pair of sites we evaluate elevation of the PSC over the level of statistical significance provided by the surrogate data test similarly as it is shown for the ordinary coherence in Fig. 6. If positive, this value quantifies the degree of synchrony between the cortical sites taking into account the dynamics observed at the other electrodes. Fig. 7 shows the degree of synchrony calculated over ICA- and wICA-corrected EEG relative to the coherence level in the control conditions. No line connecting two cortical sites means perfect concordance with control conditions, whereas red or blue links point to hiper- or hipo-connections over control conditions, respectively. ICA data processing in general leads to hiperconnectivity over all frequency bands (see also Fig. 6). Application of wICA significantly improves prediction providing only a few spurious light links in the Theta and Alpha bands.
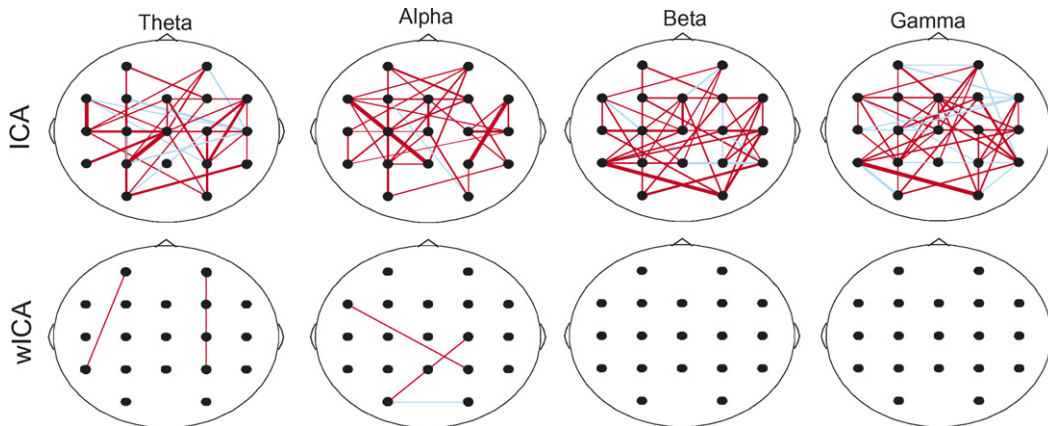
Fig. 7. Relative degree of coupling between cortical areas evaluated using partial spectral coherence. As a reference (zero level) we use the coherence evaluated at control conditions. Red and blue lines show spurious hiper- and hipo-coherence links, respectively. The link width defines the strength of the relative association between corresponding sites. (For interpretation of the references to color in this figure legend, the reader is referred to the web version of the article.)

To give a clue on the problem of biasing to the hiperconnectivity after ICA artifact suppression (Fig. 7) let us consider a case when signals of neural origin from two electrodes, $r_j(t)$ and $r_k(t)$, are statistically unrelated, and consequently have vanishing cross-correlation and coherence. We assume the signals to be corrupted by ocular artifacts, $a(t)$. An application of ICA gives:

$$\hat{x}_k(t) = r_k(t) - m_{k1}n(t), \qquad \hat{x}_j(t) = r_j(t) - m_{j1}n(t), \qquad (15)$$

where similar to (6) hatted variables correspond to ICA-corrected EEG signals, $r_{j,k}(t)$ are the artifact free signals, and $n(t) = s_1(t) - a(t)$ is the neural activity persistent in the independent component responsible for artifacts. From (15) we immediately see that although the artifact free signals $r_j(t)$ and $r_k(t)$ are uncorrelated their ICA counterparts $\hat{x}_j$ and $\hat{x}_k$ correlate due to the presence of the common term $n(t)$. Hence we have nonvanishing, spurious coherence (Appendix A):

$$|SC(\omega)| = \frac{m_{k1}m_{j1}P_{nn}}{\sqrt{P_{\hat{x}_k\hat{x}_k}P_{\hat{x}_j\hat{x}_j}}} \geq 0. \qquad (16)$$

Thus when the residual neural activity in the component identified as corresponding to artifacts is not vanishing, the spectral coherence (and partial spectral coherence as well) can be overestimated after ICA artifact suppression (Fig. 7). wICA algorithm recovers the neural activity persisting in the component, so improving results of the coherence estimation.

4. Conclusions and discussion

Recent efforts on the artifact removal in EEG recordings has shown a great utility of ICA signal decomposition. Although the success of ICA is encouraging, it should be treated with caution (Stone, 2002). Existing studies have focused almost exclusively on the important reduction of the spectral presence of typical artifacts in ICA-corrected EEGs [see, e.g. (Tong et al., 2001; Tran et al., 2004)], while distortions of the cerebral part of EEGs introduced by the method as a side effect have been left unattended. Recently, there has appeared a few quantitative studies pointing to a possible spectral distortion of the cerebral activity due to ICA correction procedures (Wallstrom et al., 2004; Kierkels et al., 2006). Meanwhile, quantification of distortions of non-local characteristics (e.g. spectral coherence) was completely lacking in the literature.

In this paper we have pursued two complimentary goals: (1) study quantitatively how suppression of artifacts in EEG data distorts the underlying cerebral activity and affects the quality of derived local and non-local characteristics; (2) propose a novel method that enhances the performance of the conventional ICA by reducing the EEG distortions due to artifact removal.

First, we have shown that ICA-corrected EEG may partially lose the cerebral activity. Indeed, ICA decomposes EEG into components of artificial and neural origins and rejects the former. Such a separation is valid for independent, linearly mixed sources when their total number does not exceed the number of recording electrodes (Bell and Sejnowski, 1995). In practice these assumptions can be violated leading to a "leak" of the

cerebral activity into components deemed artificial. Complete rejection of such a component supposes a partial loss of the neural signal. To reduce the distortions in corrected EEG we have proposed a wavelet enhanced ICA (wICA) method that allows recovering the cerebral activity leaked into the artificial components.

wICA is based on ICA signal decomposition and includes as an *intermediate* step the wavelet thresholding of the independent components. This step recovers the low amplitude, broad band neural activity persistent in the components identified as responsible for artifacts. Thus, the subsequent deletion of only the artifactual part of the components does not distort the underlying neural activity in the wICA-corrected EEG. Note that wICA not only recovers the cerebral activity outside of the artifact episodes, but also it allows substantial recovering of the neural signal under artifacts. Another advantage of wICA is its automation. No laborious, ambiguous visual inspection of the independent components is required. Instead, all components are passed through the thresholding procedure and thus only the high magnitude artifacts (e.g. from eye blinking) are cut out. At this point we recall that the proposed use of wavelet analysis not on raw EEG but on the independent components has the following important advantage. Artifacts are concentrated in a few components, where the ratio artifact magnitude to cerebral activity magnitude is much higher than in the artifact affected electrodes. This strongly improves the quality of artifact detection, and also simplifies the method application as a fine tuning of the threshold value is not required.

Second, we have quantified the performance of the ICA and wICA artifact suppression methods in the time and frequency domains using semi-simulated and real EEG recordings. Note that quantification of the quality of signal recovering refers to control, artifact free EEG. In the time domain we have shown that ICA effectively (by 19.4 dB) eliminates the presence of ocular artifacts and reduces moderately the heart beat artifacts (by 3.5 dB). wICA offers significant improvements reducing by 35.0 and 13.7 dB the presence of ocular and heart beat artifacts, respectively. In the frequency domain, we have shown that ICA tends to underestimate the EEG power spectrum over all frequency bands. We have estimated theoretically the power spectrum loss and shown that it is a product of the spectrum of the persistent neural activity and corresponding weight of the mixing matrix. This for instance means that spectral loss for ocular artifact suppression is higher in the frontal sites. Calculating the absolute value of the spectral distortion in FP1 electrode we found for ICA/wICA: 4.4/0.7, 3.8/0.2, 4.3/0.1 and 4.8/0.1 dB in the Theta, Alpha, Beta and Gamma bands, respectively.

EEG recording is a multichannel technique that provides a natural basis for the study of non-local cerebral dynamics and cortical circuitry. For the first time we have addressed the question of how the artifact suppression affects the evaluation of the simplest non-local characteristics, i.e. spectral and partial spectral coherences. Our results suggest that ICA-corrected EEGs may exhibit an overestimated level of coherence, while wICA overcomes this problem approaching the coherence level

found in the control conditions. The overestimation may lead to erroneous conclusions on the presence of spurious couplings (associations) between the corresponding cortical areas. Indeed, we have shown that the connectivity pattern provided by partial spectral coherence evaluated over ICA-corrected EEG is much more dense than in the control conditions. wICA solves the problem showing practically the same connectivity pattern as in the control conditions.

Acknowledgments

Appendix A. Derivation of spectral and coherence distortions

By definition, the power spectrum of a signal $v(t)$ is given by the Fourier transform of its autocovariance function $C_{vv}(\tau) = \langle v(t)v(t-\tau) \rangle$:

$$P_{vv}(\omega) = \int C_{vv}(\tau)\,e^{-i\omega\tau}\,d\tau. \tag{A.1}$$

Using representation (6) of the ICA cleaned EEG signal at j-th electrode we obtain its autocovariance:

$$C_{\hat{x}_j\hat{x}_j}(\tau) = C_{r_jr_j}(\tau) - 2m_{j1}C_{r_jn}(\tau) + m_{j1}^2 C_{nn}(\tau), \tag{A.2}$$

where C_{yz} denotes the covariance function of signals $y(t)$ and $z(t)$. The covariance of artifact free signal $r_j(t)$ and the residual neural activity $n(t)$ can be represented as:

$$C_{r_jn}(\tau) = C_{\hat{x}_js_1}(\tau) - C_{\hat{x}_ja}(\tau) + m_{j1}C_{nn}(\tau). \tag{A.3}$$

Now we note that (to a first approximation) the artifact does not correlate with the neural activity $C_{\hat{x}_ja}(\tau) = 0$, and the components are independent $C_{\hat{x}_js}(\tau) = 0$. Then Eq. (A.3) reduces to $C_{r_jn}(\tau) = m_{j1}C_{nn}(\tau)$. Substituting this to (A.2) and using (A.1) we obtain the spectrum of the ICA-cleaned EEG:

$$P_{\hat{x}_j\hat{x}_j}(\omega) = P_{r_jr_j}(\omega) - m_{j1}^2 P_{nn}. \tag{A.4}$$

From (A.4) the spectrum distortion given by Eq. (13) follows.

Similarly to (A.4), the cross spectrum of two EEG signals (15) cleaned by ICA is:

$$P_{\hat{x}_j\hat{x}_k}(\omega) = P_{r_jr_k}(\omega) - m_{j1}m_{k1}P_{nn}. \tag{A.5}$$

Then using the definition of spectral coherence (1), and signal representation (15) we obtain:

$$SC_{\hat{x}_j\hat{x}_k}(\omega) = \frac{P_{r_jr_k}(\omega) - m_{j1}m_{k1}P_{nn}}{\sqrt{P_{\hat{x}_j\hat{x}_j}(\omega)P_{\hat{x}_k\hat{x}_k}(\omega)}}. \tag{A.6}$$

By the assumption the cross spectrum $P_{r_jr_k}(\omega) = 0$ and we end up with (16).

References

Alegre M, Labarga A, Gurtubay I, Iriarte J, Malanda A, Artieda J. Movement-related changes in cortical oscillatory activity in ballistic, sustained and negative movements. Exp Brain Res 2003;148:17–25.

Amari S, Cichocki A, Yang H. A new learning algorithm for blind source separation. Adv Neural Inf Process Syst 1996;8:757–763.

Anemüller J, Sejnowski T, Makeig S. Complex independent component analysis of frequency—domain electroencephalographic data. Neural Networks 2003;16:1311–1323.

Bell A, Sejnowski T. An information-maximization approach to blind separation and blind deconvolution. Neural Comput 1995;7:1129–1159.

Bendat J, Piersol A. Random data: analysis and measurement procedures. New York: Wiley; 1986.

Brillinger D. Time series, data analysis and theory. San Francisco: Holden Day; 1981.

Brown G, Yamada S, Sejnowski T. Independent component analysis at the neural cocktail party. Trends Neurosci 2001;1:54–63.

Debnath L. Wavelet transforms and their applications. Birkhauser; 2002.

Delorme A, Jung C, Sejnowski T, Makeig S. Improved rejection of artefacts from EEG data using high order statistic and independent component analysis.

Delorme A, Makeig S. EEGLAB: an open source toolbox for analysis of single-trial EEG dynamics including independent component analysis. J Neurosci Meth 2004;134:9–21.

Donoho DL, Johnstone IM, Kerkyacharian G, Picardi D. Wavelet shrinkage: asymptopia?. J R Stat Soc 1995;B57:301–369.

Flexer A, Bauer H, Pripfl J, Dorffner G. Using ICA for removal of ocular artifacts in EEG recorded from blind subjects. Neural Networks 2005;18:998–1005.

Friston K. Modes or models: a critique on independent component analysis for fMRI. Trends Cogn Sci 1998;2:373–375.

Goelz H, Jones R, Bones P. Wavelet analysis of transient biomedical signals and its application to detection of epileptiform activity in the EEG. Clin Electroenc 2000;31:181–191.

Hori H, Aiba M, He B. Spatio-temporal cortical source imaging of brain electrical activity by means of time-varying parametric projection filter. IEEE Trans Biomed Eng 2004;51:768–777.

Hyvärinen A, Pajunen P. Nonlinear independent component analysis: existence and uniqueness results. Neural Networks 1999;12:209–219.

Iriarte J, Urrestarazu E, Valencia M, Alegre M, Malanda A, Viteri C, et al. Independent component analysis as a tool to eliminate artifacts in EEG: a quantitative study. J Clin Neurophysiol 2003;20:249–257.

James C, Gibson O. Temporally constrained ICA: an application to artifact rejection in electromagnetic brain signal analysis. IEEE Trans Biomed Eng 2003;50:1108–1116.

James C, Hesse C. Independent component analysis for biomedical signals. Physiol Meas 2005;26:15–39.

James CJ, Lowe D. Extracting multisource brain activity from single EM channel. Artif Intell Med 2003;28:89–104.

Jarvis M, Mitra P. Sampling properties of the spectrum and coherency of sequences of action potentials. Neural Comput 2001;134:717–749.

Joyce C, Gorodnitsky I, Kutas M. Automatic removal of eye movement and blink artifacts from EEG data using blind component separation. Psychophysiology 2004;41:313–325.

Jung T, Humphries C, Lee T, McKeown M, Iragui V, Makeig S, et al. Removing electroencephalographic artifacts by blind source separation. Psychophysiology 2000;37:163–178.

Jung T, Makeig S, Westerfield M, Townsend J, Courchesne E, Sejnowski T. Removal of eye activity artifacts from visual event-related potentials in normal and clinical subjects. Clin Neurophysiol 2000;11:1745–1758.

Kierkels J, Boxtel G, Vogten L. A model-bases objective evaluation of eye movement correction in EEG recordings. IEEE Trans Biomed Eng 2006;53:246–253.

Korzeniewska A, Manczak M, Kaminski M, Blinowska K, Kasicki S. Determination of information flow direction among brain structures by a modified directed transfer function (dDTF) method. J Neurosci Meth 2003;125:195–207.

Lee T, Girolomi M, Sejnowski T. Independent component analysis using an extended infomax algorithm for mixed subgaussian and supergaussian sources. Neural Comput 1999;11:417–441.

Makinen V, May P, Tiitinen H. Spectral characterization of ongoin and auditory event-related brain process. Neurol Clin Neurophysiol 2004;3:104.

Mallat S. A wavelet tour of signal processing. San Diego: Academic Press; 1998.

McKeown M, Jung T, Makeig S, Brown G. Spatially independent activity patterns in functional magnetic resonance imaging data during the stroop color-maming task. Proc Natl Acad Sci USA 1998;3:803–810.

Melissant C, Ypma A, Frietman E, Stam C. A method for detection of alzheimer's disease using ICA-enhanced EEG measurements. Artif Intell Med 2005;33:209–222.

Mochimaru F, Fujimoto Y, Ishikawa Y. The fetal electrocardiogram by independent component analysis and wavelet. Jpn J Physiol 2004;54:457–463.

Mormann F, Fell J, Axmancher N, Weber B, Lehnertz K, Elger C, et al. Phase/amplitude reset and theta-gamma interaction in the human medial temporal lobe during a continous word recognition memory task. Hippocampus 2005;15:890–900.

Murata A. An attempt to evaluate mental workload using wavelet transform of EEG. Hum Factors 2005;47:498–508.

Percival D, Walden AT. Spectral analysis for physical applications. Cambridge University Press; 1993.

Privik R, Broughton R, Coppola R, Davidson R, Fox N, Nuwer M. Guidelines for the recording and quantitative analysis of electroencephalographic activity in research contexts. Psychophysiology 1993;30:547–558.

Quiroga R, Garcia H. Single-trial event-related potentials with wavelet denoising. Clin Neurophysiol 2003;114:376–390.

Rodriguez E, George N, Lachaux JP, Martinerie J, Renault B, Varela F. Perception's shadow: long-distance synchronization of human brain activity. Nature 1999;397:430–433.

Rong-Yi Y, Zhong C. Blind source separation of multichannel electroencephalogram based wavelet transform and ICA. Chinese Phys 2005;14:2176–2180.

Schiff S, Aldroubi A, Unser M, Sato S. Fast wavelet transformation of EEG. Electroencephal Clin Neurophysiol 1994;91:442–455.

Schreiber T, Schmitz A. Surrogate time series. Physica D 2000;142:646–652.

Stone JV. Independent component analysis: an introduction. Trends Cogn Sci 2002;6:59–64.

Theiler J, Eubank S, longtin A, Galdrikian B, Farmer D. Testing for nonlinearity in time series: the method of surrogate data. Physica D 1992;58:77–94.

Thomson D. Spectrum estimation and harmonic analysis. Proc IEEE 1982;70:1055–1096.

Tong S, Bezerianos A, Paul J, Zhu Y, Thakor N. Removal of ECG interference from the EEG recordings in small animals using independent component analysis. J Neurosci Meth 2001;108:11–17.

Tran Y, Craig A, Boord P, Craig D. Using independent component analysis to remove artifact from electroencephalographic measured during stuttered speech. Med Biol Eng Comput 2004;42:627–633.

Urrestarazu E, Iriarte J, Alegre M, Valencia M, Viteri C, Artieda J. Independent component analysis removing artifacts in ictal recordings. Epilepsia 2004;45:1–8.

Varela F, Lachaux JP, Rodriguez E, Martinerie J. The brainweb: phase synchronization and large-scale integration. Nat Rev Neurosci 2001;2:229–238.

Vigario R. Extraction of ocular artifats from EEG using independent component analysis. Electroencephal Clin Neurophysiol 1997;103:395–404.

Vigario R, Särelö J, Jousmäki V, Hämäläinem H, Oja E. Independent component approach to the analysis of EEG and MEG recordings. IEEE Trans Biomed Eng 2000;47:589–593.

von Stein A, Rappelsberger P, Sarnthein J, Petsche H. Synchronization between temporal and parietal cortex during multimodal object processing in man. Cerebral Cortex 1999;9:137–150.

Wallstrom G, Kass R, Miller A, Cohn J, Fox N. Automatic correction of ocular artifacts in the EEG: a comparison of regression-based and component-based methods. Int J Psychophysiol 2004;53:105–119.

Wan X, Iwata K, Riera J, Ozaki T, Kitamura M, Kawashima R. Artifact reduction for EEG/fMRI recordings: nonlinear reduction of ballistocardiogram artifacts. Clin Neurophysiol 2006;117:1–13.